ELSEVIER

Contents lists available at ScienceDirect

Journal of Membrane Science

journal homepage: www.elsevier.com/locate/memsci



Mechanism of pore wetting in membrane distillation with alcohol vs. surfactant



Zhangxin Wang^{a,1}, Yuanmiaoliang Chen^{a,1}, Xiangming Sun^a, Ravindra Duddu^a, Shihong Lin^{a,b,*}

ABSTRACT

Pore wetting is a unique and important technical challenge that can lead to process failure in membrane distillation (MD) using hydrophobic membranes. While it is well known that both low-surface-tension and water miscible liquids, such as alcohols, and amphiphilic molecules, such as surfactants, are effective wetting agents, the detailed mechanisms for these agents to induce pore wetting remain unclear. In particular, the role of surface adsorption in surfactant-induced wetting remains to be elucidated. This study provides fundamental insights to understanding the mechanism of pore wetting induced by these two different wetting agents. Using a recently developed wetting monitoring technique based on single-frequency transmembrane impedance, we experimentally probe the kinetics of wetting frontier propagation. We demonstrate that ethanol-induced wetting is instantaneous whereas surfactant-induced wetting is dynamic with its kinetic rate dependent on several critical factors. We also develop a theoretical model, based on the assumption of quasi-equilibrium adsorption, to successfully explain the important features experimentally observed in surfactant-induced wetting. Specifically, it was found that the kinetics of surfactant-induced wetting strongly depends on the vapor flux and the bulk concentration of surfactants in the feed solution, but surprisingly not on the transmembrane hydraulic pressure difference. The results from our study also suggest that while the presence of surfactants promotes wetting. adsorption of surfactants onto pore surface actually deters pore wetting instead of promoting it by rendering the surface hydrophilic.

1. Introduction

Membrane distillation (MD) is a thermal desalination technology capable of using low-temperature heat to desalinate hypersaline water [1-6]. In an MD process, a microporous hydrophobic membrane is applied to separate a hot salty stream, known as feed solution, and a cold distillate stream. Air pockets are trapped within such a membrane because the membrane hydrophobicity prevents the feed solution and distillate from intruding into the membrane pores. Driven by the partial water vapor pressure difference resulting from the temperature difference of the two streams, water evaporates from the feed solution, transports across the air pockets, and condenses to become part of the distillate. The hydrophobic membrane thereby serves as a barrier to prevent the salty feed stream from passing through the membrane in its liquid form and mixing with the distillate. MD has several major technological advantages, including the capability of utilizing lowgrade energy, the ability to treat hypersaline wastewaters, small system footprint, and low capital cost due to the absence of high pressure and

high temperature components [7–15].

In spite of all its advantages, MD has not been widely applied in industry, likely due to several major technical challenges. One of the major technical challenges that limit the application of MD is membrane pore wetting [16-18]. Membrane pore wetting refers to the penetration of feed water through the membrane pores and the consequent failure of MD operation due to the compromised salt rejection rate. Previous studies have shown that the presence of low-surfacetension (LST) or amphiphilic agents in the feed solution induces pore wetting in MD with hydrophobic membranes [19-22]. Recent studies have explored both material and operational solutions to this technical challenge. Specifically, the development of omniphobic membranes has been shown to be a promising material solution [19,23-25]. Alternatively, composite membranes with a hydrophilic coating have been shown to enhance wetting resistance [26,27]. On the other hand, a combined material and operational approach using superhydrophobic membrane with air-layer recharging has also proven to be a viable solution [22,28].

^a Department of Civil and Environmental Engineering, Vanderbilt University, Nashville, TN 37235-1831, United States

b Department of Chemical and Biomolecular Engineering, Vanderbilt University, Nashville, TN 37235-1831, United States

^{*} Corresponding author at: Department of Chemical and Biomolecular Engineering, Vanderbilt University, Nashville, TN 37235-1831, United States. E-mail address: shihong.lin@vanderbilt.edu (S. Lin).

¹ These two authors contributed equally to this work.

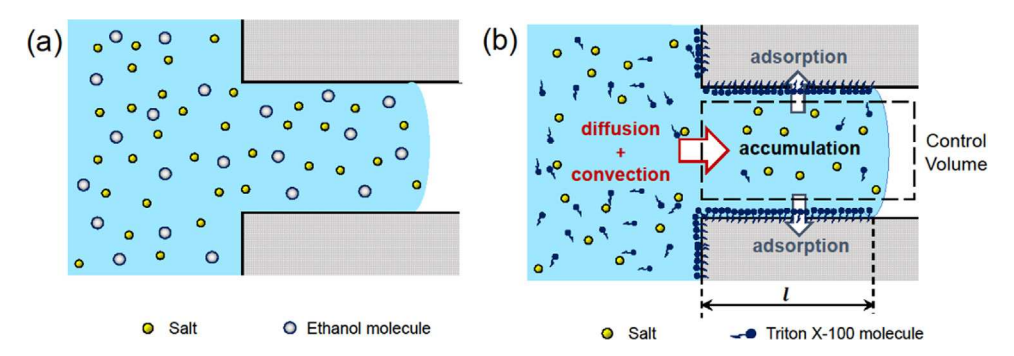


Fig. 1. Illustration of wetting of a cylindrical pore by saline feed solutions containing (A) ethanol and (B) Triton X-100. For pore wetting induced by ethanol, the solution enters the membrane pore when the transmembrane pressure exceeds the LEP. Adsorption of ethanol molecules onto the pore surface is negligible. For pore wetting by Triton X-100 solution, the liquid-air interface (i.e. the wetting frontier) propagates forward toward the distillate when the transmembrane pressure exceeds the LEP corresponding to the Triton X-100 concentration at the liquid-air interface. Triton X-100 in the feed solution inside the

pores are constantly removed by the pore surface via adsorption, which tends to reduce the surfactant concentration and increase the LEP at the liquid-air interface. The kinetics of interface propagation is therefore controlled by the kinetics of surfactant adsorption.

Despite all these efforts in addressing the challenge of pore wetting in MD, the exact mechanism of pore wetting has yet to be thoroughly elucidated. It is generally believed that wetting occurs if the transmembrane hydraulic pressure difference exceeds the liquid entry pressure (LEP) that depends on membrane material, pore structure, and the surface tension of the feed solution. This theoretical framework can explain pore wetting induced by lowering the surface tension of the feed solution via addition of LST and water miscible liquid, such as alcohol, into the aqueous feed solution. However, when surfactants are used to promote pore wetting, it is unclear if wetting occurs simply because surfactants reduce the surface tension of the feed solution, or because the pore surface becomes hydrophilic due to surfactant adsorption. While the first mechanism is certainly important, the second mechanism also sounds probable and has been suggested by several studies to be a possible contribution [21,29]. However, if the first mechanism is the sole contribution to pore wetting, a testable hypothesis is that feed solutions containing LST liquid and surfactants should behave similarly in inducing pore wetting, as long as their surface tension is adjusted to be the same. Differentiating these mechanisms requires more advanced techniques for probing wetting dynamics which is inaccessible by simply monitoring salt rejection.

Recently, a novel technique based on single-frequency impedance measurement has been developed for monitoring the dynamics of pore wetting in MD [29]. Unlike the conventional method of measuring distillate salinity, which can detect wetting only if some membrane pores have been fully penetrated by the feed solution, the impedance-based technique is capable of detecting the dynamic movement of the liquid-air interface (i.e. the wetting frontier) even if no pore has been wicked through and no change in distillate salinity has occurred. The forward propagation of the wetting frontier toward the distillate is the precursor of imminent wetting and a key feature of wetting dynamics.

In this study, we comparatively investigate the behaviors of pore wetting in direct contact membrane distillation (DCMD) with feed solutions containing two different types of wetting agents. The first wetting agent, ethanol, is a LST and non-adsorbing liquid miscible with water. The second wetting agent, Triton X-100, is a charge-neutral surfactant. Using a novel wetting monitoring technique based on single-frequency impedance measurement, we study the dynamic wetting of polyvinylidene fluoride (PVDF) membranes in DCMD experiments to elucidate the fundamental difference between wetting induced by ethanol and by surfactant. We also develop a novel theoretical model to describe the dynamics of surfactant-induced pore wetting, and use DCMD experiments to verify several key predictions from such a model regarding the impacts of surfactant concentration, feed temperature, and transmembrane hydraulic pressure on wetting kinetics.

2. Theory and model development

2.1. General criterion of pore wetting

The minimum transmembrane pressure difference required for liquid to intrude into a membrane pore is the liquid entry pressure (LEP) as given by Eq. (1):

$$LEP = -\frac{2B\gamma_L \cos\theta}{r} \tag{1}$$

where γ_L is the liquid surface tension, θ is the intrinsic liquid contact angle between the liquid and the solid membrane material, r is the equivalent pore radius, and B is the geometric factor accounting for the non-cylindrical pore geometry and assumes unity for perfect cylindrical pores. The addition of wetting agents, regardless of chemical compositions, reduces γ_L of the feed solution, thereby decreasing LEP and facilitating pore wetting. [2,21,23,30,31] We note that the change of γ_L also affects θ , as the intrinsic contact angle depends on both γ_L and the surface energy of the solid material. In this sense, γ_L and $\cos\theta$ can be grouped into one single parameter, $\gamma_L \cos\theta$, because they cannot vary independently as γ_L changes.

Both alcohol and surfactants can reduce γ_L , $cos\theta$, and consequently, $\gamma_L cos\theta$. However, the fundamental difference between these two wetting agents is that the surface energy of the solid pore surface can be modified by surfactants via surface adsorption (Fig. 1b) but not by simple alcohols which is hardly surface active (Fig. 1a). Is it possible, then, that surface adsorption is one of the reasons for pore wetting induced by surfactants, because the membrane pores are rendered hydrophilic by the adsorbed surfactants? This mechanism of pore wetting induced by surfactant adsorption has indeed been suggested in literature [21,29,32]. However, we contend here with two arguments that surface adsorption of surfactants unlikely has positive contribution to pore wetting.

First, surface adsorption of surfactants is possible only when the surfactant-containing feed solution is already in contact with the solid surface, in which case the solid surface has already been wetted by definition. In other words, it is improbable that surfactants can adsorb onto the non-wetted area of the solid surface and render it hydrophilic. Altering the surface energy of the already-wetted region of a solid surface has little relevance to whether the non-wetted portion of a surface can be wetted by the surfactant solution or not, i.e. the relevant surface energy that should be used in Eq. (1) is the intrinsic surface energy of the membrane material, not that of the surfactant-modified surface. The second argument regards the ability of omniphobic membrane to resist wetting by surfactant solution [19,23-25]. According to well-established theory, omniphobicity is attainable only if the surface has both low surface energy and reentrant structure [33-35]. If surface hydrophilization were indeed a mechanism for surfactant-induced pore wetting, omniphobic membrane should not have wetting resistance to surfactant solutions, which is inconsistent

with experimental observations [19,23,36]. Therefore, surfactant adsorption should not contribute positively to pore wetting. On the contrary, surfactant adsorption deters pore wetting by surfactant-containing solutions in MD, as we will explain below.

Now we assume that surface hydrophilization by surfactant adsorption is not a positive contribution to membrane pore wetting, the general criterion of pore wetting is simply that ΔP is higher than LEP according to the general criterion of wetting [2,21]:

$$\Delta P > LEP$$
 (2)

The reason of using ΔP instead of just the feed hydraulic pressure when comparing with LEP has been elucidated in literature [37] and summarized in Appendix A.

This general criterion should apply to wetting induced by both alcohols and surfactants. However, we note that the LEP should be calculated based on the solution properties of the wetting frontier but not those of the bulk solution. This is of particular importance for surfactant-induced wetting, as adsorption of surfactants reduces the surfactant concentration at the wetting frontier and leads to a frontier LEP that may be much higher than that of the bulk solution.

2.1.1. Membrane wetting by alcohol solution

For wetting of an ideal cylindrical pore by feed solution containing ethanol (Fig. 1 a), which is non surface active, the kinetics of propagation of the wetting frontier toward the distillate can be modeled by treating the solution within a pore as an expanding Poiseuille flow [38,39]. In this case, the wetting kinetics is described by Eq. (3) (detailed derivation shown in Appendix B):

$$l(t) = \sqrt{\frac{r^2}{4\mu}(\Delta P - LEP)t}$$
(3)

where l is the intrusion depth defined as the distance between the wetting frontier and the pore entrance, r is the pore radius, μ is the dynamic viscosity of the feed solution, and t is the time since feed solution enters the pore. The function l(t) describes the time-dependent position of the wetting frontier, which can be semi-quantitatively probed by measuring the transmembrane impedance [29].

2.1.2. Membrane wetting by surfactants

Albeit pore wetting by surfactant solution should follow the same general criterion given by Eq. (2), its wetting dynamics differs drastically from that of alcohol-induced wetting due to the strong adsorption of surfactant onto the pore surface (Fig. 1b). The relevant LEP for the propagation of the wetting frontier (i.e. the liquid-air interface) depends on the interfacial concentration of surfactants, which is in turn controlled by the transport of surfactants to the wetting frontier. On the one hand, adsorption of surfactants onto the pore surface surrounding the wetting frontier tends to reduce the surfactant concentration, which in turn tends to increase γ_L at the wetting frontier and retards further wetting. On the other hand, diffusion of surfactants down concentration gradient and convection induced by transmembrane vapor flux, both in the axial direction of the pore, replenish the surfactants at the wetting frontier, which in turn tend to decrease γ_L and further promote wetting.

Theoretically, we can solve a partial differential equation (PDE) regarding the diffusion-convection-adsorption of surfactants to obtain the spatiotemporal distribution of surfactant concentration in the water column within a partially wetted pore (Appendix C). One key boundary condition is that the surfactant concentration at the wetting frontier is such that the corresponding LEP equals ΔP . In addition, the spatial boundary for the PDE, which is the position of the wetting frontier, constantly changes as interface continuously propagates toward the distillate. The goal of solving the PDE is to quantify the position of the shifting boundary as a function of time, i.e., l(t). The numerical solution of such a PDE of a time-dependent boundary condition is challenging to obtain, and more importantly, provides limited intuitive insight to understanding the dynamics of surfactant-induced pore wetting. Here,

we present a simplified quasi-equilibrium-adsorption model with which we can derive a simple analytical approximation of l(t) that captures the most important features of surfactant-induced dynamic wetting.

Two primary simplifying assumptions are applied in our derivation. First, it can be shown that the longitudinal diffusive contribution to surfactant transport is negligible compared to the convective contribution (Appendix D). Second, we assume that adsorption is very fast compared to longitudinal surfactant transport so that local adsorption equilibrium is reached at any moment, i.e., the local surface concentration of surfactants, $\tau(x)$, can be determined by the local aqueous surfactant concentration, c(x), following an adsorption isotherm. This assumption of quasi-equilibrium-adsorption is a reasonable approximation because (1) the mean radial diffusion distance, i.e., the mean distance for which surfactant molecules travel radially before they adsorb onto the pore surface, is roughly the membrane pore size and thus very small compared to l(t) except at the beginning of wetting; and (2) physical adsorption of surfactants via hydrophobic interaction involves no specific chemical interaction that requires activation energy, and is therefore not rate-limiting.

To describe the adsorption equilibrium, we first consider the Langmuir isotherm which is widely applied for monolayer adsorption as in the case of surfactant adsorption. The Langmuir isotherm is given by

$$\tau(x) = \tau_{max} \frac{Kc(x)}{1 + Kc(x)} \tag{4}$$

where τ_{max} is the maximum area density of Triton X-100 (surfactant to be used in this study) on pore surface and K is an equilibrium constant that governs the partition of Triton X-100 between the membrane surface and the solution phase. Here, we consider an MD membrane made of (PVDF) for obtaining the parameters in Eq. (4). With the Triton X-100 concentration used in this study and the relevant K value reported in literature for PVDF [40], it can be shown that $Kc(x) \gg 1$, which reduces the Langmuir isotherm to a stepwise adsorption isotherm employed in the previous literature [39]:

$$\tau(x) = \begin{cases} \tau_{max}, & c(x) > 0 \\ 0, & c(x) = 0 \end{cases}$$
 (5)

Eq. (5) implies that, as long as the PVDF surface is in equilibrium with a Triton X-100 solution of a non-trivial concentration, the surface will always be fully saturated by the Triton X-100 molecules. Consequently, if the PVDF surface has not yet been fully saturated, which is the case for the differential portion of the pore surface surrounding the wetting frontier, the aqueous concentration of Triton X-100 in equilibrium with such an unsaturated part of the surface should approach zero. In other words, the wetting frontier is depleted of surfactants due to the continuous and fast removal of surfactants from the solution via adsorption onto the pore surface near the frontier. As a result, the γ_L of the wetting frontier is close to the γ_L of surfactant-free water due to the very low interfacial surfactant concentration. Therefore, wetting frontier does not proceed toward the distillate until its surrounding pore surface is fully saturated with surfactant molecules that are constantly replenished to the wetting frontier by axial convection. In other words, the wetting kinetics is mostly controlled by the kinetics of convective transport of Triton X-100 molecules to the wetting frontier.

The mass balance for surfactants in a partially wetted pore, including both the feed solution and the wetted PVDF surface, is expressed by Eq. (6).

$$vc_0 t\pi r^2 = \int_0^{l(t)} \left[\tau_{max} 2\pi r (1-\varepsilon) + c(x)\pi r^2 \right] dx$$
 (6)

where c_0 is the concentration of Triton X-100 in the bulk solution outside the membrane pore, and ν is the convective flow velocity, which is approximately equal to vapor flux, J, divided by porosity, ε (i.e. $\nu = J/\varepsilon$). Specifically, the term on the left-hand-side represents the total amount of Triton X-100 entering the pore from time zero to t, considering only convection. The first part of the integral on the right-

hand-side quantifies the amount of Triton X-100 adsorbed onto the pore surface that has been already wetted, with the factor $1-\varepsilon$ accounting for the fact that a typical pore wall (except for those in a track-etched membrane) is fragmented in the axial direction and membrane porosity is assumed to be isotropic. The second part of the integral represents the amount of Triton X-100 in the aqueous solution in the partially wetted pore. According to previous literature [41,42], τ_{max} is estimated to be 3 \times 10⁻⁶ mol m⁻² for Triton X-100 adsorption on PVDF, rendering the second term in the integral 6 negligible compared to the first term. Therefore, Eq. (6) can be simplified as

$$l(t) \approx \frac{r}{2\varepsilon (1-\varepsilon)\tau_{max}} Jc_0 t \tag{7}$$

Eq. (7) suggests that for given membrane and surfactant, in which case r, ε , and τ_{max} are constant, the kinetic rate of wetting frontier propagation is proportional to the feed surfactant concentration, c_0 , and to vapor flux, J. Remarkably, Eq. (7) also implies that the kinetics of wetting does not depend on ΔP , except when ΔP is too high that it exceeds the LEP of surfactant-free feed solution. These unique dependences of wetting kinetics on c_0 , J, and ΔP can be readily and reliably tested using MD experiments.

3. Materials and methods

3.1. Materials

The hydrophobic PVDF membrane with a nominal pores size of 0.45 μm was purchased from GE Healthcare (Pittsburg, PA). Sodium chloride (NaCl), Triton X-100, and ethanol (200 proof) were all procured from Sigma Aldrich (St. Louis, MO) and used without further purification.

3.2. Surface tension measurements

The surface tensions of aqueous NaCl solution (0.6 M) with different concentrations of ethanol and Triton X-100 were measured at 60 $^{\circ}$ C by analyzing the shape of a submerged air bubble in a given solution using an optical tensiometer (TL100, Attension, Finland) with drop shape analysis software [43–45]. Additionally, the surface tensions of 50 ppm Triton X-100 in NaCl aqueous solutions at temperatures of 40, 50, 60, and 70 $^{\circ}$ C were also measured.

3.3. Impedance-based monitoring of wetting in MD experiments

The experimental setup for direct contact MD (DCMD) experiments is similar to those used in many previous studies [7,29,46] and is briefly described in Appendix E. We also employ a recently developed wetting monitoring technique based on real time measurement of single-frequency impedance. The major advantage of this impedance-based technique is that it can capture the transition state of wetting in which some pores are partially wetted but no pore has yet been fully penetrated (Fig. 2). In contrast, the conventional approach of wetting monitoring based on measuring distillate salinity is responsive only if some of the pores have been fully penetrated through. The impedance-based technique provides much more insights for probing the dynamic propagation of wetting frontier.

For each DCMD wetting experiment, prior to the addition of wetting agent (ethanol or Triton X-100), the system was operated with feed solution (0.6 M NaCl aqueous solution) free of wetting agent for half an hour to establish baselines of flux and impedance. Water flux, distillate conductivity, and transmembrane impedance (at $100\,\mathrm{kHz}$ frequency) were constantly monitored. Five different sets of DCMD wetting experiments were conducted. The first set of experiments compared wetting induced by ethanol solution and by Triton X-100 solution with the same surface tension. The second set of experiments was designed to study the impact of ΔP in wetting induced by ethanol. The third and

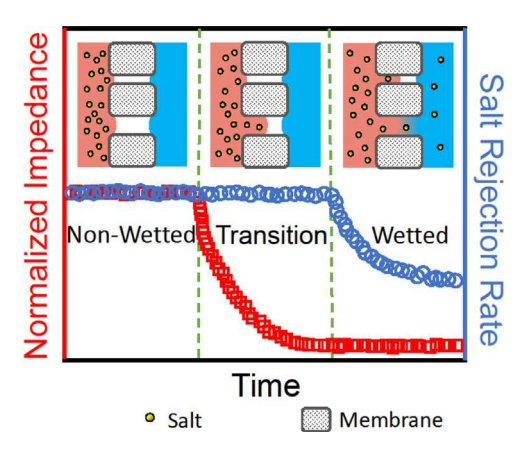


Fig. 2. Representative data of normalized transmembrane impedance (red squares) and salt rejection (blue circles, based on distillate salinity measurement). In the non-wetted state, the transmembrane impedance was stable and the salt rejection was perfect. In the transition state (i.e. the feed solution has entered some pores but has not penetrated through any pore), the impedance declines due to the decreased air gap between the feed solution and distillate, whereas the salt rejection still remains perfect. In the wetted state (i.e. the solution has completely penetrated some, if not all, of pores), the salt rejection starts to decline, whereas the normalized transmembrane impedance approaches zero.

fourth sets of experiments were performed to investigate the influences of surfactant concentration and vapor flux in membrane wetting induced by Triton X-100, respectively. The last set of experiments was conducted to show the effect of ΔP on surfactant-induced wetting.

When interpreting the measured impedance, the MD membrane can be considered as equivalent to a parallel circuit of a capacitor and a resistor [29,47,48]. At high frequencies, the capacitive contribution dominates the transmembrane admittance (i.e. reciprocal of impedance). Therefore, the impedance is roughly proportional to the thickness of the remaining air gap. The time-resolved transmembrane impedance normalized by the initial transmembrane impedance can thus provide a semi-quantification of the wetting frontier position following Eq. (8) (Appendix F):

$$\frac{Z(t)}{Z_0} = \frac{d_0 - l(t)}{d_0} \tag{8}$$

Where, Z_0 is the initial transmembrane impedance, Z(t) is the transmembrane impedance at time t, d_0 is the thickness of the membrane which was 180 μ m for the membrane used in this study.

4. Results and discussion

4.1. Triton X-100 vs. ethanol as a wetting agent: drastically different wetting behaviors

Representative data of transmembrane impedance (red squares) and salt rejection (blue circles) in DCMD wetting experiments with Triton X-100 or ethanol as wetting agent are shown in Fig. 3. When Triton X-100 was used as wetting agent (Fig. 3a), the transmembrane impedance responded to pore wetting much earlier than the salt rejection based on distillate salinity measurement, thanks to the ability of impedance-based technique to probe the propagation of the wetting frontier before any pore has been fully wetted through [29]. For membrane wetting caused by ethanol, the transmembrane impedance and salt rejection rate responded almost simultaneously and the wetting was instantaneous (Fig. 3b). The wetting occurred so fast that it required almost no time, after the addition of ethanol, for the feed solution to fully wick through the pores.

For the two experiments shown in Fig. 3, the surface tension of the feed solutions after adding Triton X-100 or ethanol were controlled to

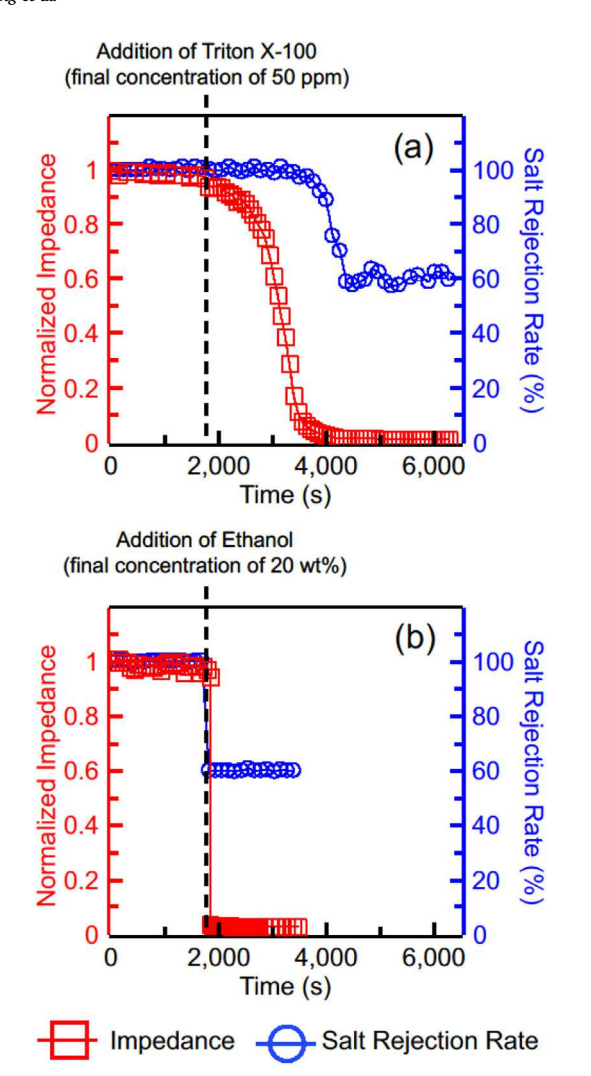


Fig. 3. Impedance (red squares, left Y-axis) across the PVDF membrane and salt rejection (blue circles, right Y-axis) in DCMD experiments in the presence of (a) 50 ppm Triton X-100 and (b) 20 wt% ethanol solution. The impedances are normalized by the initial impedance (4299 Ω in panel a, and 4439 Ω in panel b). In both DCMD experiments, 0.6 M NaCl solution and DI water were used as the feed and distillate streams, respectively. The temperatures of the feed and distillation streams were kept at 60 and 20 °C, respectively. The transmembrane hydraulic pressure was set at 5 kPa. The black dash line indicates the addition of wetting agent (Triton X-100 in panel a, and ethanol in panel b) to the feed solution, which resulted in a feed solution with surface tension of around 35 mN/m according to the surface tension measurements data (Fig. A4 in Appendix G). The water flux data corresponding to the experiments are shown in Fig. A5 in Appendix H.

be approximately the same (\sim 35 mN/m, Appendix G), despite the drastically different wetting behaviors observed. Whereas wetting induced by ethanol was instantaneous, wetting induced by Triton X-100 was gradual and dynamic. The dynamic behavior of surfactant-induced wetting is attributable to the adsorption of Triton X-100 to the membrane pore surface which constantly removes the amphiphilic wetting agent from the wetting frontier and thereby slows down the wetting process. In contrast, because ethanol does not adsorb onto the membrane pore surface (even if it does, adsorption would barely change bulk ethanol concentration which is very large), as long as ΔP exceeds LEP, pore wetting occurs at a kinetic rate following the Poiseuille flow. Using Eq. (3) with the experimental conditions, the time for complete wetting is estimated to be less than 1 s (Appendix B), which is in accordance with the experimentally observed instantaneity of ethanol-induced wetting.

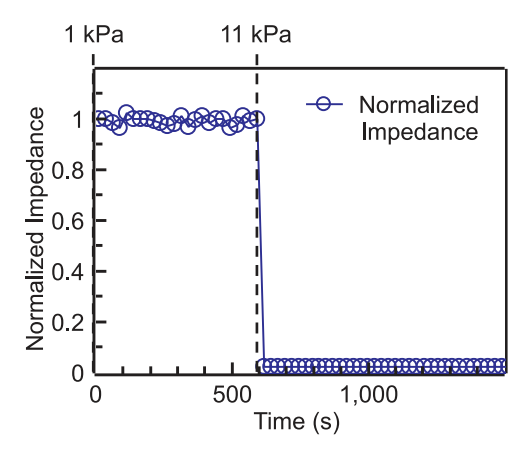


Fig. 4. Experimentally measured transmembrane impedance with feed solution containing ethanol. The transmembrane hydraulic pressure was changed from 1 kPa (before the dash line) to 11 kPa (at and after the dash line). The impedances are normalized by the initial impedance which was $4854\,\Omega$. The ethanol concentration of the feed solution was $15\,\text{wt}\%$. The temperatures of feed and distillate streams were set at 60 and $20\,^{\circ}\text{C}$, respectively. The water flux and salt rejection are shown in Fig. A6 in Appendix H.

4.2. Ethanol-induced wetting: a simple application of the general wetting criterion

When ethanol was employed as the wetting agent, we can simply apply the general wetting criterion given by Eq. (2) using the LEP of the bulk solution: if ΔP is lower than LEP, membrane wetting does not occur; if ΔP is higher than LEP, wetting occurs instantly. The experiment shown in Fig. 3b is an example of inducing wetting via lowering the LEP by reducing the surface tension of the feed solution via adding ethanol. When the surface tension of the feed solution was low enough, LEP became lower than ΔP , which led to instant and complete pore wetting. Alternatively, one can also induce wetting by increasing ΔP to an extent that it surpasses the LEP of all pores. For example, we conducted an MD wetting experiment with a saline feed solution containing 15 wt% ethanol using different transmembrane hydraulic pressures (Fig. 4). The results suggest that an MD membrane that was not wetted with $\Delta P = 1$ kPa was immediately fully wetted as soon as ΔP was raised to 11 kPa. The results on Fig. 3b and Fig. 4 both demonstrate that, for ethanol-induced wetting, one can simply determine if wetting can occur using Eq. (2) with the LEP of bulk solution.

4.3. Surfactant-induced wetting: a dynamic process limited by surfactant transport

When surfactants are employed to induce wetting in MD, more complex dynamic wetting occur due to the adsorption of surfactants onto the pore surface. By treating surfactant transport and adsorption as a pseudo-steady-state processes, we have developed a simplified model that describes the kinetics of wetting frontier propagation (Eq. (7)) which predicts several key features of surfactant-induced wetting. Here, using Triton X-100 as the model surfactant, we experimentally assess these key features and verify their consistence with Eq. (7). Specifically, we want to evaluate whether the model summarized in Eq. (7) can, at least qualitatively, predict the impacts of several key factors on the kinetics of surfactant-induced wetting. The kinetics of wetting frontier propagation can be semi-quantitatively approximated by the transmembrane impedance using the following equation obtained simply by combining Eqs. (7) and (8):

$$\frac{Z(t)}{Z_0} = 1 - \frac{R}{2\varepsilon (1 - \varepsilon)\tau_{max} d_0} Jc_0 t \tag{9}$$

Eq. (9) suggests that the rate of impedance decline is proportional to vapor flux, J, and the feed concentration of surfactants, c_0 . It also

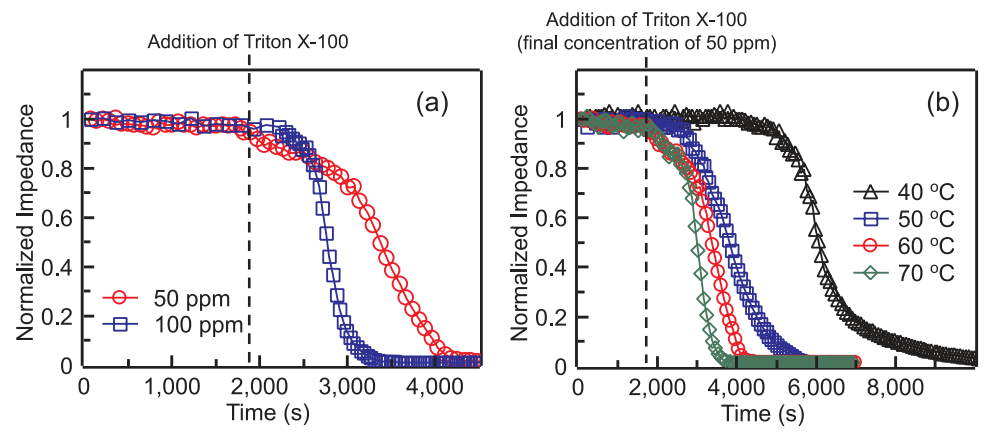


Fig. 5. (a) Experimentally measured impedances across the PVDF membrane in DCMD experiments in the presence of 50 ppm Triton X-100 (red circles) and 100 ppm Triton X-100 (blue squares) in the feed solutions. The impedances are normalized by the initial impedances which were 4299 and 4199 Ω for experiments with feed solutions containing 50 ppm ethanol and 100 ppm Triton X-100, respectively. The temperatures of feed and distillate streams were kept 60 and 20 °C, respectively. (b) Experimentally measured impedances across the PVDF membrane in DCMD experiments with different fluxes resulting from different feed temperatures. With a constant distillate temperature of 20 °C, the feed temperatures were set at 40 °C (black trian-

gles), 50 °C (blue squares), 60 °C (red circles) and 70 °C (green diamonds) to yield vapor fluxes of 8.60, 17.69, 29.95, and $47.13 \, Lm^{2} h^{-1}$, respectively. The measured impedances are normalized by the initial impedances which were 5007, 4480, 4299 and 3329 Ω for experiments with feed temperatures of 40 °C, 50 °C, 60 °C and 70 °C, respectively. In all panels, the black dash lines indicate the additions of Triton X-100 to the feed solutions. The resulting Triton X-100 concentration in panel (b) was 50 ppm. The transmembrane hydraulic pressure was kept at 5 kPa in all experiments. The water fluxes and salt rejections corresponding to the experiments are shown in Figs. A7 and A8 in Appendix H.

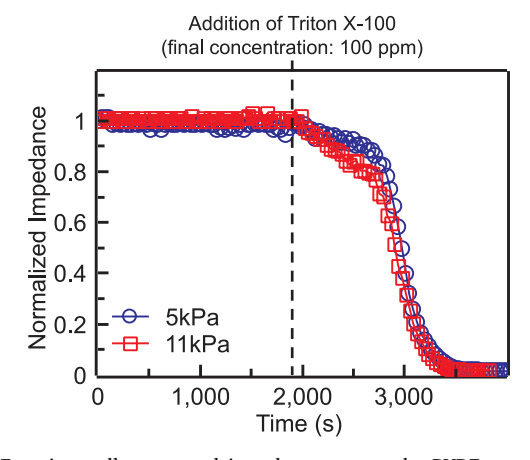


Fig. 6. Experimentally measured impedances across the PVDF membrane in DCMD experiments with transmembrane hydraulic pressures of 5 kPa (blue circles) and 11 kPa (red squares). The impedances are normalized by the initial impedances which were 4270 and 4377 Ω for experiments with transmembrane pressures of 5 kPa and 11 kPa, respectively. The black dash line indicates the addition of Triton X-100 to the feed solution which yielded a Triton X-100 concentration of 100 ppm. The vapor flux was controlled to be around 30 LMH by adjusting the feed temperatures to account for the different hydrodynamic impacts resulting from having different feed pressures. The vapor flux and salt rejection in these experiments are shown in Fig. A9 in Appendix H.

implies, rather surprisingly, that ΔP , does not have a direct impact on wetting kinetics, which we will elaborate later. While Eq. (9) suggests a linear decline of normalized transmembrane impedance, we note that such linearity results from a highly simplified model with the ideal assumptions that the membrane pores are perfectly cylindrical and of a uniform size and that diffusive contribution to overall surfactant transport is negligible. Because these ideal assumptions, which are required to derive Eq. (9), are most certainly not satiated with any realistic MD membrane, we do not expect to apply Eq. (9) for accurate quantitative prediction of experimental results. Rather, we want to experimentally assess the semi-quatitative dependence of impedance decline rate on critical operating parameters such as c_0 , J and ΔP .

For wetting experiments with different Triton X-100 concentrations in feed solutions (Fig. 5a), it was observed that the impedance decline was significantly faster with a feed solution of a higher Triton X-100 concentration (100 ppm, blue squares) than with a feed solution of a lower surfactant concentration (50 ppm, red circles), which is semi-quantitatively consistent with Eq. (9). Based on the developed model,

the wetting frontier does not proceed unless its surrounding pore surface has been fully saturated with the adsorbed surfactants. For multiple factors that have been discussed in the model development section, the kinetics of Triton X-100 adsorption around the wetting frontier is limited by how fast the surfactants are replenished via convection from the bulk solution to the wetting frontier. Since the rate of convective transport is primarily determined by c_0 and J, a higher bulk concentration of surfactants leads to a faster wetting process.

For the similar reason, the wetting kinetics also positively correlates with vapor flux, J. To show this, a set of MD wetting experiments were conducted to achieve different vapor fluxes by adjusting feed temperature. Specifically, the measured vapor fluxes with a constant distillate temperature of 20 °C but different feed temperatures at 40, 50, 60, and 70 °C were 8.60, 14.97, 29.97, and 47.13 L m $^{-2}$ h $^{-1}$ respectively. The experimental results (Fig. 5b) shows a positive correlation between vapor flux and wetting kinetics. It is worth noting that changing the temperature from 50 to 70°C does not significantly affect the surface tension of the feed solution with 50 ppm Triton X-100: the measured surface tensions of the solution are 32.5 \pm 0.5, 32.4 \pm 0.4, 32.9 \pm 0.8, 32.2 \pm 0.9 mN/m at 40 °C, 50 °C, 60 °C and 70 °C, respectively. Therefore, the primary impact of feed temperature on the wetting kinetics was realized mostly via the enhanced vapor flux.

One counterintuitive prediction from Eq. (9) is that the rate of surfactant-induced pore wetting is independent of the ΔP . This theoretical prediction is particularly surprising especially considering that the general wetting criterion solely compares the ΔP with LEP regardless of the chemical nature of the wetting agent. Nonetheless, controlled wetting experiments with all other parameters maintained the same except for different ΔP yielded results that support the theoretical prediction (Fig. 6). Pore wetting in experiments with two very different transmembrane pressures (5 and 11 kPa) was both progressive instead of instantaneous, which is characteristic of surfactant-induced wetting, and has remarkably similar kinetics of impedance decline.

The insensitivity of wetting kinetics to ΔP can be interpreted in the following way. Let us apply the general wetting criterion stipulated by Eq. (2) and assume a critical condition that wetting frontier moves forward as long as $\Delta P = LEP$. Here, LEP is defined not based on the property of the bulk feed solution, but rather on the property of the solution at the wetting frontier which has a surfactant concentration significantly lower than the bulk concentration. Due to the dependence of γ_L on surfactant concentration and the dependence of LEP on γ_L , there exists a specific surfactant concentration at the wetting frontier that corresponds to a specific LEP. Let us define the critical surfactant concentrations at the wetting frontier with which wetting occurs with a

 ΔP of 5 kPa and 11 kPa as c_A' and c_B' , respectively, with the superscript emphasizing the concentrations are defined for the wetting frontier but not the bulk solution. From Eqs. 1 and 2, together with the dependence of γ_L on Triton X-100 concentration (Fig. A4b), it can be readily shown that c_A' is significantly lower than c_B' . However, the adsorption isotherm given by Eq. (4) suggests that, regardless of the aqueous Triton X-100 concentration (except when it is very close to zero), the equilibrium surface concentration of the adsorbed Triton X-100 should always be roughly equal to the maximum surface concentration, τ_{max} , which can also be mathematically written as

$$\tau(c_A') \approx \tau(c_B') \approx \tau_{max}$$
 (10)

In other words, a lower critical concentration of surfactants at the wetting frontier does not lead to a lower equilibrium surface concentration of the adsorbed surfactants on the pore surface near the wetting frontier. In any case, the aqueous surfactant concentration at the wetting frontier cannot increase to the critical concentration required for forward propagation of the frontier until the surrounding pore surface is almost fully saturated with the adsorbed surfactants. Therefore, the wetting kinetics is eventually controlled by the rate at which pore surface is saturated by the adsorbed surfactants, which is in turn controlled by the rate at which surfactants are transported to wetting frontier via convection. Transmembrane hydraulic pressure has relatively little significance in determining wetting kinetics because it has no impact on neither the convective transport nor the adsorption of surfactants.

The only exceptional scenario in which ΔP will play a role is when it becomes higher than the LEP of a surfactant-free feed solution (significantly higher than 100 kPa). In this case, ΔP is always higher than the LEP of the feed solution, regardless of the surfactant concentration at the wetting frontier. Wetting will become instantaneous, similar to ethanol-induced wetting. However, this is a rather trivial scenario in the current context because wetting of such kind is not really induced by surfactants.

5. Conclusion

Pore wetting is a failure mechanism unique to MD, and at the same time, a technical challenge that limits the applications of MD. Unlike membrane fouling, which is a common failure mechanism across different membrane processes, pore wetting in MD has been understood to a significantly lesser extent. This study provides new fundamental insights to understanding MD pore wetting and elucidates the mechanism of surfactant-induced wetting. Specifically, we demonstrate the fundamental difference between wetting induced by surfactants and by alcohols, and show that the two drastically different phenomena share the same simple underlying wetting principle.

Ethanol wetting is instant as long as ΔP exceeds the LEP. In comparison, surfactant-induced wetting is dynamic, with its kinetic rate strongly dependent on several factors that affect the kinetics of surfactant adsorption to pore surface. Both theoretical model and experimental results suggest that bulk concentration of surfactants and water vapor flux in MD have strong impacts on the wetting kinetics. Notably, a surprising yet justifiable feature of surfactant-induced wetting is that its kinetics is mostly independent of transmembrane hydraulic pressure.

While the current study provides new and mechanistic insights to understanding MD pore wetting, the conclusions from this study may not be universally applicable to all pore wetting phenomena in MD. In particular, compared to pore wetting induced by highly effective wetting agents, pore wetting in many practical MD processes involving mineral scaling or fouling by natural organic matter occurs in much lower rates and may involve different mechanisms. Future work is needed to further elucidate wetting in those more complicated and longer-term scenarios before we can arrive in a comprehensive understanding of pore wetting in MD.

Acknowledgements

The authors are grateful to the National Science Foundation for its support via Grants CBET 1705048 and CBET 1739884.

Appendix A. Justification of using transmembrane hydraulic pressure instead of feed hydraulic pressure for wetting analysis

See Appendix Fig. A1

In this analysis, we present the proof that the transmembrane hydraulic pressure, ΔP , instead of the hydraulic pressure of the feed stream, should be used to compared with LEP as a criterion for pore wetting. Such a proof was first given by Zmievskii [37] and is simply summarized here. We start with conducting a force balance analysis on the water and air trapped in an ideal cylindrical pore between the feed solution and the distillate (Fig. A1).

Let us assume that the hydraulic pressure on the feed side, P_f , is higher than that on the distillate side, P_d , so that ΔP is always positive. The force balance for the feed solution and distillate within the pore can be described by the two following equations:

$$P_f \pi r^2 = P_{air} \pi r^2 + (-\cos \theta_f) \gamma_f 2\pi r \tag{A1}$$

$$P_d \pi r^2 = P_{air} \pi r^2 + (-\cos\theta_d) \gamma_d 2\pi r \tag{A2}$$

where r is the radius of the membrane pore; P_{air} is the pressure of air trapped in the membrane pore; θ_f and θ_p are the intrinsic contact angles of the feed solution and the distillate on the membrane material, respectively; γ_f and γ_p are the surface tensions of the feed solution and distillate,

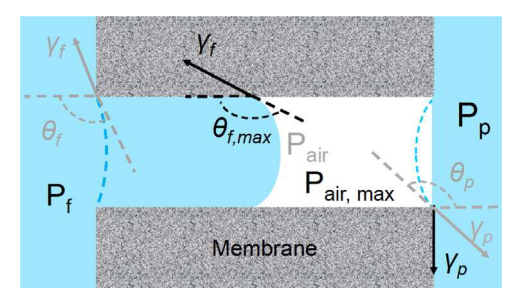


Fig. A1. Schematic of membrane pore wetting in DCMD. P_f and P_p are the applied hydraulic pressures on the feed and distillatesides, respectively. P_{air} is the pressure of the trapped air in the membrane pore. γ_f and γ_p are the surface tensions of the feed solution and distillate (or permeate), respectively. θ_f and θ_p are the contact angles of the feed solution and distillate on the PVDF membrane surface, respectively.

respectively

When feed solution has not yet intruded into the membrane pore, increasing P_f first increases θ_f . But P_{air} remains constant because the increasing curvature of feed/air interface barely changes the volume of the air trapped in the pore. Based on Eq. (A1), the increased hydraulic pressure on the feed solution is balanced by the increased interfacial force caused by an increased θ_f . As P_f further increases, θ_f will reach a maximum, $\theta_{f,max}$, that is determined by the surface tensions of the feed solution and membrane material. Further increasing P_f will lead to intrusion of the feed solution into the pore, which will in turn compress the air trapped in the pore and increase its pressure.

Once the air pressure starts to increases, force balance on the distillate (Eq. (A2)) dictates that θ_d decreases because P_{air} increases yet P_d remains constant. As P_{air} continues to increase, θ_d will become less than zero and an air bubble will emerge in the distillate until θ_d reaches -90° . Further increase of P_{air} will cause detachment of air bubble, which will result in destabilization of the system and complete pore wetting. At this critical point of pore wetting, Eq. (A1) and (A2) can be combined to obtain Eq. (A3), with $\theta_f = \theta_{f,max}$ and $\theta_d = -90^\circ$:

$$(P_f - P_p)\pi r^2 = (-\cos\theta_{f,max})\gamma_f 2\pi r \tag{A3}$$

Rearranging Eq. (A3) yields Eq. (A4):

$$\Delta P = P_f - P_p = \frac{-2\gamma_f}{r} \cos\theta_{f,max} = LEP \tag{A4}$$

Eq. (A4) suggests that at the critical point of pore wetting, LEP should be equal to the transmembrane hydraulic pressure difference, ΔP , not the feed hydraulic pressure, P_f . Therefore, the criterion for pore wetting is that $\Delta P > LEP$.

Appendix B. Derivation of Eq. (3)

According to Poiseuille equation [49,50],

$$\Delta P - LEP = \frac{8\mu lQ}{\pi r^4} \tag{A5}$$

where ΔP is the applied transmembrane pressure, LEP is the liquid entry pressure of the membrane pore, l is the distance between the wetting frontier and the pore entrance, μ is the dynamic viscosity, Q is the volumetric flow rate (i.e. $Q = \pi r^2 \frac{dl}{dt}$), r is the pore radius. Rearranging Eq. (A5) gives

$$ldl = \frac{(\Delta P - LEP)r^2}{8\mu}dt \tag{A6}$$

Integrating Eq. (A6) from l = 0 to l, and t = 0 to t, we can obtain,

$$\frac{l^2}{2} = \frac{(\Delta P - LEP)r^2}{8\mu}t\tag{A7}$$

We can obtain Eq. (A8), which is Eq. (3) in the main text, from rearranging Eq. (A7)

$$l(t) = \sqrt{\frac{r^2}{4\mu}(\Delta P - LEP)t}$$
(A8)

In our experiments, $r = 0.225\mu m$, $\mu = 0.47mPa \cdot s$, for $\Delta P - LEP = 0.25kPa$, which is a very small pressure difference, the time t it takes for the liquid to penetrate through the entire membrane ($l(t) = d_0$, where the membrane thickness $d_0 = 180\mu m$) is calculated to be 1.22s.

Appendix C. Partial differential equation for surfactant transport

The partial differential equation regarding the diffusion-convection-adsorption of surfactant within a partially wetted pore [39] is given by

$$\frac{\partial c}{\partial t} + \frac{2}{r} \frac{\partial \tau}{\partial t} = D \frac{\partial^2 c}{\partial x^2} \tag{A9}$$

where c (abbreviation for c(x, t)) is the concentration of surfactants at position x, and time t, τ is the surface concentration of the surfactant on the pore surface, r is the pore radius, D is the diffusion coefficient of surfactants in the solution, D is the vapor flux, E is the porosity of the membrane, D is the moving speed of the wetting frontier (D is D in our experiments). The initial conditions for the equation is C (D is the surfactant concentration in the bulk solution. The boundary condition at the pore entrance is C (D is D in the boundary condition at the wetting frontier is D is the critical concentration of surfactant that satisfies D is D in the surface concentration of the surfactant on the surface concentration of the surface con

Appendix D. Relative insignificance of axial diffusion

See Appendix Fig. A2

According to literatures [41,51,52], $D=4\times10^{-7}cm^2s^{-1}$, and the adsorption occurs so fast that the pore surface would be saturated immediately as the solution is in contact with the pore surface $(\frac{\partial \tau}{\partial t}=0 \text{ for } c\neq 0)$. We can solve a specific case of the PDE at steady state with $J=14\,\mathrm{L\,m^{-2}\,h^{-1}}$ (relatively low), $c_0=0.08mM$, $c^*=0$ (the extreme case), and $l=30\mu m$ (less than 20% of the membrane thickness). The result is plotted in Fig. A1. In this specific case, the diffusion term at the pore entrance, $D\frac{dc}{dx}\big|_{x=0}$, is only 3.22% of the convection term, Jc_0 . This suggests that except for the beginning of the wetting when l is very short, axial diffusion is relatively insignificant compared to convection for surfactant transport, and can thus be numerically ignored. When a higher J or/and c_0 , the axial diffusion at the pore entrance will become even more negligible compared to convection.

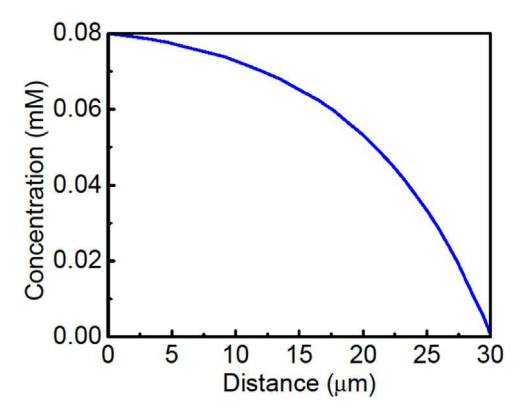


Fig. A2. The concentration profile of Triton X-100 in the solution for $l=30\mu m$. In this specific case, the bulk concentration $c_0=0.08mM$, the critical concentration $c^*=0$, the diffusion coefficient $D=4\times 10^{-7}cm^2s^{-1}$, and the vapor flux with J=14 L m $^{-2}$ h $^{-1}$.

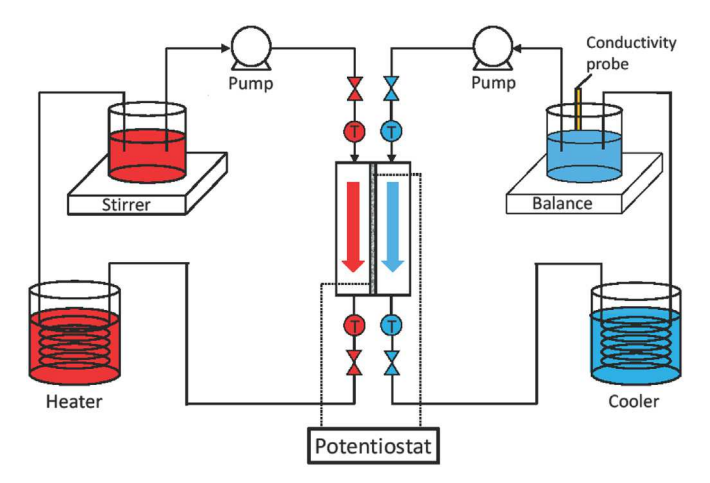


Fig. A3. Schematic of DCMD experiment coupled with a potentiostat.

Appendix E. Experimental setup

See Appendix Fig. A3

We used a direct contact membrane distillation (DCMD) experimental setup coupled with a potentiostat in our membrane wetting experiments [29]. During the experiments, the salt rejection rate was calculated based on the real time water flux and the salinity of the distillatestream, while the transmembrane impedance at 100 kHz was measured using the potentiostat. The schematic of the experimental setup is shown in Fig. A3.

Appendix F. Derivation of Eq. (8)

As the membrane is equivalent to a parallel circuit of a resistor and a capacitor, at a high frequency (100 kHz), the transmembrane impedance is approximately equal to the impedance of the capacitor. The capacitance of the capacitor *C* can be calculated as

$$C = \frac{\varepsilon_p A}{d} \tag{A10}$$

where, ε_p is the permittivity of the air, A is the area of the air, d is the distance between the two air-liquid interfaces across the membrane. The transmembrane impedance Z can be expressed as a function of capacitance and frequency, : ω

$$Z = \frac{1}{i\omega C} \tag{A11}$$

The distance d can be expressed using the membrane thickness d_0 , and the position of the wetting frontier at time t, l(t):

$$d = d_0 - l(t) \tag{A12}$$

Combining Eq. (A10) to A12 yields

$$Z = \frac{d_0 - l(t)}{i\omega\varepsilon_p A} \tag{A13}$$

Normalizing Z with Z_0 yields

$$\frac{Z}{Z_0} = \frac{d_0 - l(t)}{d_0} \tag{A14}$$

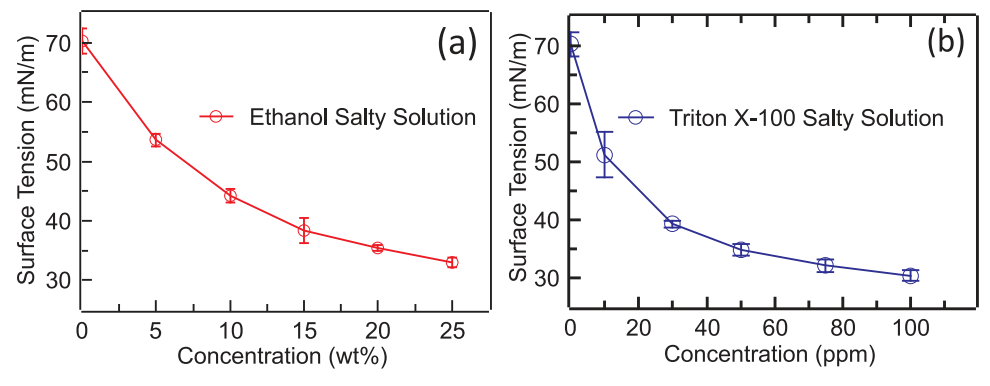


Fig. A4. The surface tensions of 0.6 M NaCl aqueous solutions with different concentrations of (a) ethanol (red circles), and (b) Triton X-100 (blue circles) at 60 °C.

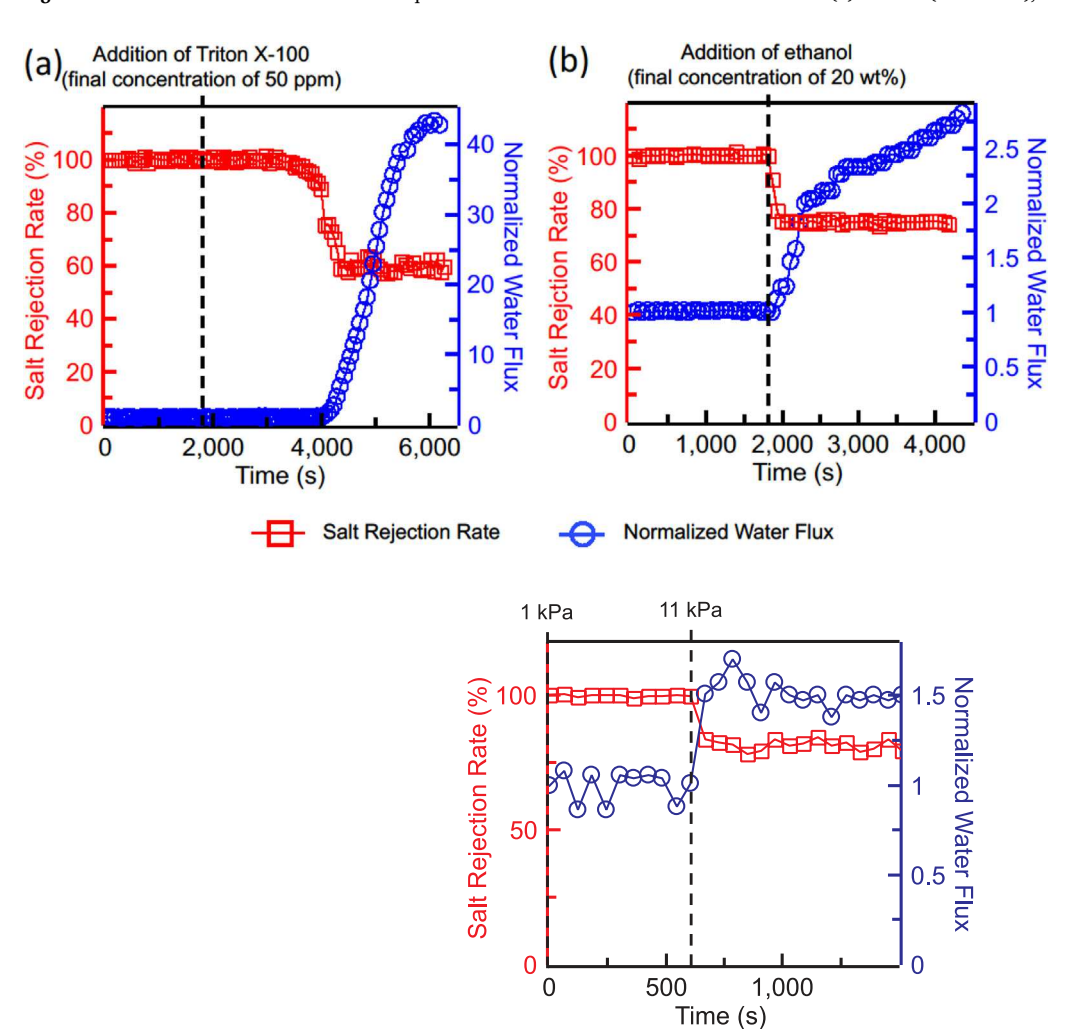


Fig. A5. Salt rejection rate (red squares, left Y-axis) and normalized water (liquid and vapor) flux (blue circles, right Y-axis) in DCMD experiments the impedance and salt rejection rate of which are reported in Fig. 3 of the main text. The water fluxes are normalized by the initial water fluxes of the respective measurements. The initial water (only vapor, no liquid) fluxes in (a) and (b) were 29.48 and 29.95 LMH, respectively.

Fig. A6. Salt rejection rate (red squares, left Y-axis) and normalized water (liquid and vapor) flux (blue circles, right Y-axis) in DCMD experiments the impedance and salt rejection rate of which are reported in Fig. 4 of the main text. The water flux is normalized by the initial water flux. The initial water (only vapor, no liquid) flux was 29 LMH.

Salt Rejection Rate Normalized Water Flux

which is Eq. (8) in the main text.

Appendix G. Surface tension measurements

See Appendix Fig. A4

The results of surface tension measurement using pedant drop method are shown in Fig. A3. Fig. A3 suggests that both the 20 wt% ethanol salty solution (red circles) and 50 ppm Triton X-100 salty solution have a surface tension of \sim 35 mN/m. Therefore, in our wetting experiments to compare

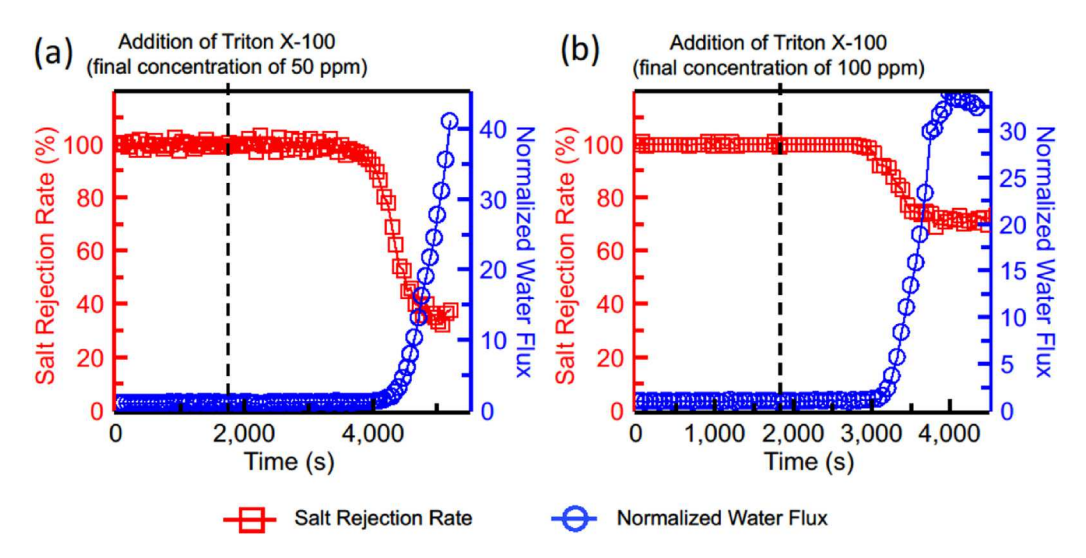


Fig. A7. Salt rejection rate (red squares, left Y-axis) and normalized water (liquid and vapor) flux (blue circles, right Y-axis) in DCMD experiments the impedance and salt rejection rate of which are reported in Fig. 5a of the main text. The water fluxes are normalized by the initial water fluxes of the respective measurements. The initial water (only vapor, no liquid) fluxes in (a) and (b) were 29.48 and 29 LMH, respectively.

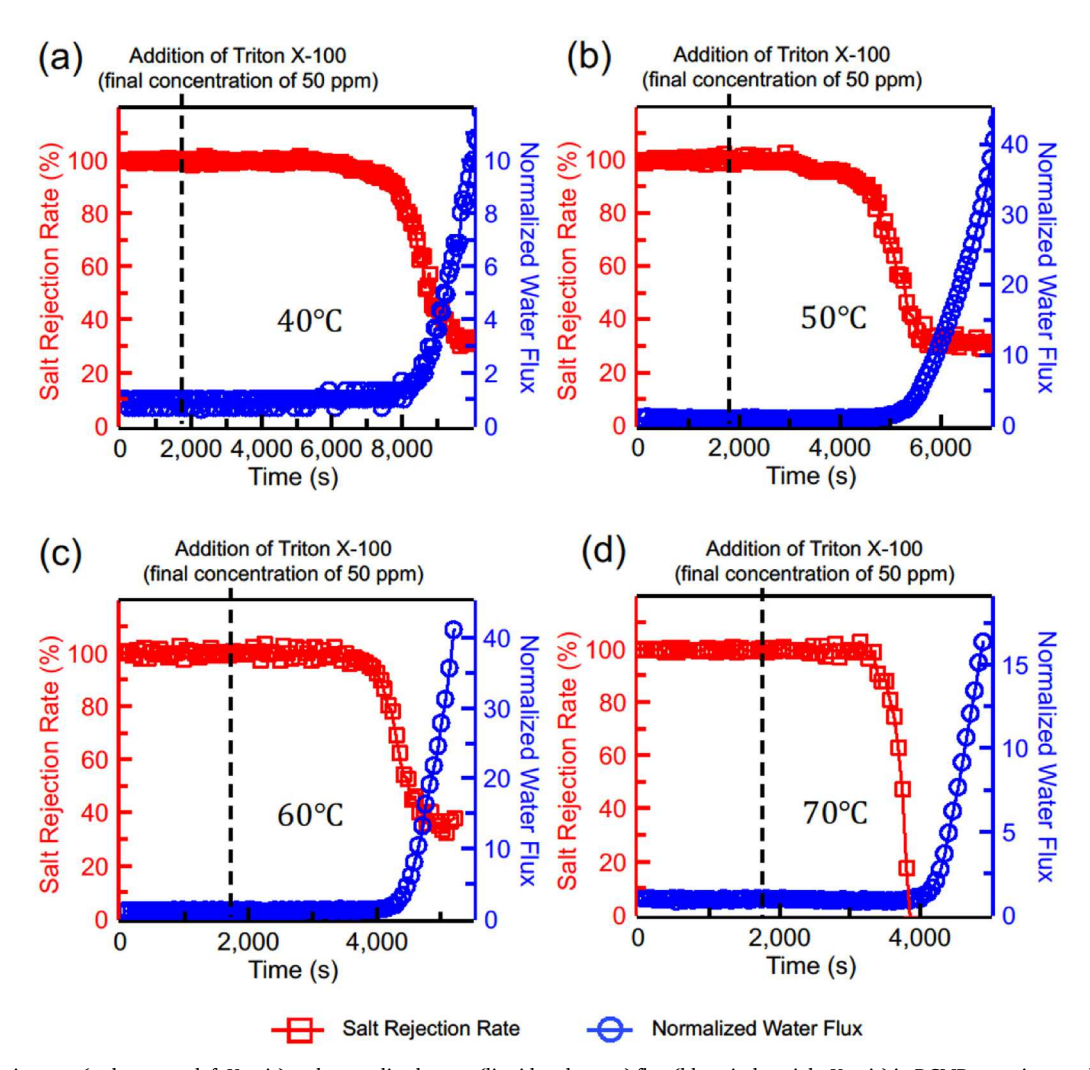


Fig. A8. Salt rejection rate (red squares, left Y-axis) and normalized water (liquid and vapor) flux (blue circles, right Y-axis) in DCMD experiments the impedance and salt rejection rate of which are reported in Fig. 5b of the main text. The water fluxes are normalized by the initial water fluxes of the respective measurements. The initial water (only vapor, no liquid) fluxes in (a) (b), (c), and (d) were 8.60, 14.97, 29.95, and 47.13 LMH, respectively.

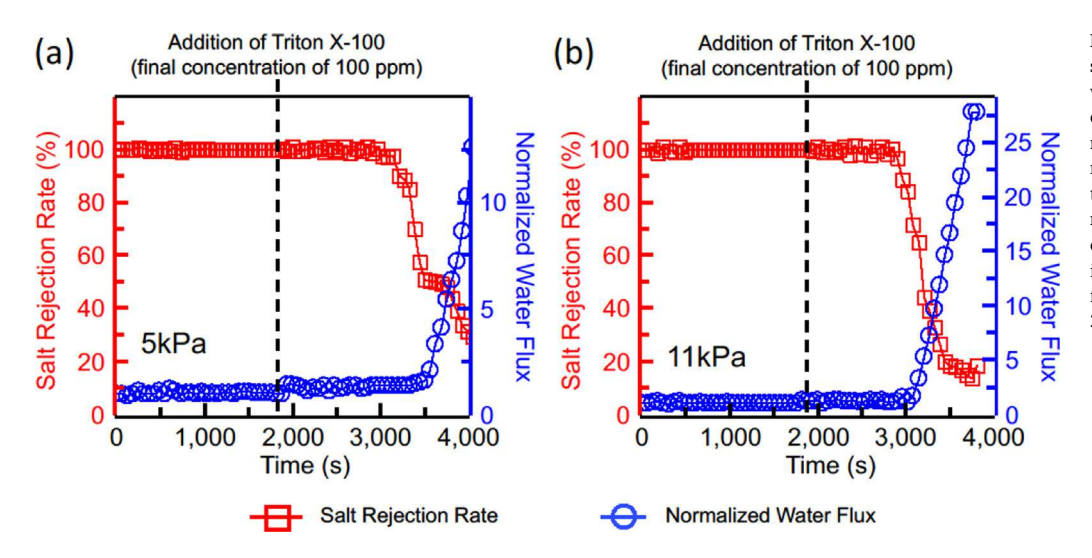


Fig. A9. Salt rejection rate (red squares, left Y-axis) and normalized water (liquid and vapor) flux (blue circles, right Y-axis) in DCMD experiments the impedance and salt rejection rate of which are reported in Fig. 6 of the main text. The water fluxes are normalized by the initial water fluxes of the respective measurements. The initial water (only vapor, no liquid) fluxes in (a) and (b) were 28.85, and 29.48 LMH, respectively.

the wetting behaviors of ethanol and Triton X-100, 20 wt% ethanol salty solution and 50 ppm Triton X-100 salty solution were chosen as the feed solutions, respectively.

Appendix H. Water flux and salt rejection rate

See Appendix Figs. A5-A9

The normalized water fluxes and salt rejection rate as functions of time in DCMD experiments are shown in Figs. A5–A9. In all DCMD experiments, the baseline normalized water flux was 1, and the initial salt rejection rate was near 100%. As the membrane became wetted, some membrane pores were fully wicked through by the feed solution, resulting in a drastically reduced salt rejection rate and significantly increased normalized water flux. The increase of normalized water flux could be attributed to the fact that the fully wicked-through membrane pores became available for convective liquid water flow. As the hydarulic pressure on the feed side was controlled to be higher than that on the distillate side, the convective water flow through the wicked-through pores was always from the feed stream to the distillate stream. Because such a hydraulic pressure driven convective water flux was significantly faster than the vapor flux driven by partial vapor pressure difference, the total water flux, as a sum of the liquid flux and vapor flux, increased as more pores became fully wicked through.

References

- [1] K.W. Lawson, D.R. Lloyd, Membrane distillation, J. Memb. Sci. 124 (1997) 1–25, http://dx.doi.org/10.1016/S0376-7388(96)00236-0.
- [2] A. Alkhudhiri, N. Darwish, N. Hilal, Membrane distillation: a comprehensive review, Desalination 287 (2012) 2–18, http://dx.doi.org/10.1016/j.desal.2011.08.
- [3] E. Drioli, A. Ali, F. Macedonio, Membrane distillation: recent developments and perspectives, Desalination 356 (2015) 56–84, http://dx.doi.org/10.1016/j.desal. 2014.10.028.
- [4] M. Khayet, T. Matsuura, J.I. Mengual, M. Qtaishat, Design of novel direct contact membrane distillation membranes, Desalination 192 (2006) 105–111, http://dx. doi.org/10.1016/j.desal.2005.06.047.
- [5] M.K. Souhaimi, T. Matsuura, Membrane Distillation: Principles and Applications, Elsevier, Amsterdam, 2011.
- [6] A. Deshmukh, C. Boo, V. Karanikola, S. Lin, A.P. Straub, T. Tong, et al., Membrane distillation at the water-energy nexus: limits, opportunities, and challenges, Energy Environ. Sci. (2018), http://dx.doi.org/10.1039/C8EE00291F.
- [7] Z. Wang, S. Lin, Membrane fouling and wetting in membrane distillation and their mitigation by novel membranes with special wettability, Water Res. 112 (2017) 38-47, http://dx.doi.org/10.1016/j.watres.2017.01.022.
- [8] F. Banat, N. Jwaied, Economic evaluation of desalination by small-scale autonomous solar-powered membrane distillation units, Desalination 220 (2008) 566–573, http://dx.doi.org/10.1016/j.desal.2007.01.057.
- [9] J. Bundschuh, N. Ghaffour, H. Mahmoudi, M. Goosen, S. Mushtaq, J. Hoinkis, Low-cost low-enthalpy geothermal heat for freshwater production: innovative applications using thermal desalination processes, Renew. Sustain. Energy Rev. 43 (2015) 196–206, http://dx.doi.org/10.1016/j.rser.2014.10.102.
- [10] Y.D. Kim, K. Thu, N. Ghaffour, K. Choon Ng, Performance investigation of a solar-assisted direct contact membrane distillation system, J. Memb. Sci. 427 (2013) 345–364, http://dx.doi.org/10.1016/j.memsci.2012.10.008.
- [11] D.L. Shaffer, L.H. Arias Chavez, M. Ben-Sasson, S. Romero-Vargas Castrillón, N.Y. Yip, M. Elimelech, Desalination and reuse of high-salinity shale gas produced water: drivers, technologies, and future directions, Environ. Sci. Technol. 47 (2013) 9569–9583, http://dx.doi.org/10.1021/es401966e.
- [12] C.R. Martinetti, A.E. Childress, T.Y. Cath, High recovery of concentrated RO brines using forward osmosis and membrane distillation, J. Memb. Sci. 331 (2009) 31–39, http://dx.doi.org/10.1016/j.memsci.2009.01.003.

- [13] T. Tong, M. Elimelech, The global rise of zero liquid discharge for wastewater management: drivers, technologies, and future directions, Environ. Sci. Technol. 50 (2016) 6846–6855, http://dx.doi.org/10.1021/acs.est.6b01000.
- [14] P.D. Dongare, A. Alabastri, S. Pedersen, K.R. Zodrow, N.J. Hogan, O. Neumann, et al., Nanophotonics-enabled solar membrane distillation for off-grid water purification, Proc. Natl. Acad. Sci. USA 114 (2017) 6936–6941, http://dx.doi.org/10.1073/pnas.1701835114.
- [15] J. Wu, K.R. Zodrow, P.B. Szemraj, Q. Li, Photothermal nanocomposite membranes for direct solar membrane distillation, J. Mater. Chem. A (2017), http://dx.doi.org/ 10.1039/C7Ta04555G
- [16] M.R. Qtaishat, T. Matsuura, 13 Modelling of pore wetting in membrane distillation compared with pervaporation. (https://doi.org/http://dx.doi.org.proxy2.library. illinois.edu/10.1016/B978-1-78242-246-4.00013-1>.
- [17] E. Guillen-Burrieza, M.O. Mavukkandy, M.R. Bilad, H.A. Arafat, Understanding wetting phenomena in membrane distillation and how operational parameters can affect it, J. Memb. Sci. 515 (2016) 163–174, http://dx.doi.org/10.1016/j.memsci. 2016.05.051.
- [18] Y. Liao, R. Wang, A.G. Fane, Engineering superhydrophobic surface on poly(viny-lidene fluoride) nanofiber membranes for direct contact membrane distillation, J. Memb. Sci. 440 (2013) 77–87, http://dx.doi.org/10.1016/j.memsci.2013.04.006.
- [19] S. Lin, S. Nejati, C. Boo, Y. Hu, C.O. Osuji, M. Elimelech, Omniphobic membrane for robust membrane distillation, Environ. Sci. Technol. Lett. 1 (2014) 443–447, http://dx.doi.org/10.1021/ez500267p.
- [20] D.M. Kargbo, R.G. Wilhelm, D.J. Campbell, Natural gas plays in the marcellus shale: challenges and potential opportunities, Environ. Sci. Technol. 44 (2010) 5679–5684, http://dx.doi.org/10.1021/es903811p.
- [21] A.C.M. Franken, J.A.M. Nolten, M.H.V. Mulder, D. Bargeman, C.A. Smolders, Wetting criteria for the applicability of membrane distillation, J. Memb. Sci. 33 (1987) 315–328, http://dx.doi.org/10.1016/S0376-7388(00)80288-4.
- [22] M. Rezaei, D.M. Warsinger, J.H. Lienhard V, W.M. Samhaber, Wetting prevention in membrane distillation through superhydrophobicity and recharging an air layer on the membrane surface, J. Memb. Sci. 530 (2017) 42–52, http://dx.doi.org/10. 1016/j.memsci.2017.02.013.
- [23] C. Boo, J. Lee, M. Elimelech, Omniphobic polyvinylidene fluoride (PVDF) membrane for desalination of shale gas produced water by membrane distillation, Environ. Sci. Technol. 50 (2016) 12275–12282, http://dx.doi.org/10.1021/acs.est. 6b03882.
- [24] C. Boo, J. Lee, M. Elimelech, Engineering surface energy and nanostructure of microporous films for expanded membrane distillation applications, Environ. Sci.

- Technol. 50 (2016) 8112-8119, http://dx.doi.org/10.1021/acs.est.6b02316.
- [25] Y.C. Woo, Y. Chen, L.D. Tijing, S. Phuntsho, T. He, J.S. Choi, et al., CF4plasma-modified omniphobic electrospun nanofiber membrane for produced water brine treatment by membrane distillation, J. Memb. Sci. 529 (2017) 234–242, http://dx.doi.org/10.1016/j.memsci.2017.01.063.
- [26] P. Peng, A.G. Fane, X. Li, Desalination by membrane distillation adopting a hydrophilic membrane, Desalination 173 (2005) 45–54, http://dx.doi.org/10.1016/j.desal 2004 06 208
- [27] X. Yang, R. Wang, L. Shi, A.G. Fane, M. Debowski, Performance improvement of PVDF hollow fiber-based membrane distillation process, J. Memb. Sci. 369 (2011) 437–447, http://dx.doi.org/10.1016/j.memsci.2010.12.020.
- [28] D.M. Warsinger, A. Servi, S. Van Belleghem, J. Gonzalez, J. Swaminathan, J. Kharraz, et al., Combining air recharging and membrane superhydrophobicity for fouling prevention in membrane distillation, J. Memb. Sci. 505 (2016) 241–252, http://dx.doi.org/10.1016/j.memsci.2016.01.018.
- [29] Y. Chen, Z. Wang, K. Jennings, S. Lin, Probing pore wetting in membrane distillation using impedance: early detection and mechanism of surfactant-induced wetting, Environ. Sci. Technol. Lett. 4 (2017) 505–510, http://dx.doi.org/10.1021/acs.ortlett.7000272
- [30] M.M.C. Garcia-Payo, M.A.M. Izquierdo-Gil, C. Fernandez-Pineda, Wetting study of hydrophobic membranes via liquid entry pressure measurements with aqueous alcohol solutions, J. Colloid Interface Sci. 230 (2000) 420–431, http://dx.doi.org/10. 1006/fcis 2000.7106
- [31] D.E.M. Warsinger, A. Servi, G.B. Connors, M.O. Mavukkandy, H.A. Arafat, K. Gleason, et al., Reversing membrane wetting in membrane distillation: comparing dryout to backwashing with pressurized air, Environ. Sci. Water Res. Technol. 3 (2017) 930–939, http://dx.doi.org/10.1039/C7EW00085E.
- [32] N.G.P. Chew, S. Zhao, C.H. Loh, N. Permogorov, R. Wang, Surfactant effects on water recovery from produced water via direct-contact membrane distillation, J. Memb. Sci. 528 (2017) 126–134, http://dx.doi.org/10.1016/j.memsci.2017.01.
- [33] A. Tuteja, W. Choi, M. Ma, J.M. Mabry, S. a Mazzella, G.C. Rutledge, et al., Designing superoleophobic surfaces, Science 318 (2007) 1618–1622, http://dx.doi. org/10.1126/science.1148326.
- [34] A.K. Kota, W. Choi, A. Tuteja, Superomniphobic surfaces: design and durability, MRS Bull. 38 (2013) 383–390, http://dx.doi.org/10.1557/mrs.2013.101.
- [35] E.J. Lee, B.J. Deka, J. Guo, Y.C. Woo, H.K. Shon, A.K. An, Engineering the re-entrant hierarchy and surface energy of PDMS-PVDF membrane for membrane distillation using a facile and benign microsphere coating, Environ. Sci. Technol. 51 (2017) 10117–10126. http://dx.doi.org/10.1021/acs.est.7b01108.
- [36] J. Lee, C. Boo, W.H. Ryu, A.D. Taylor, M. Elimelech, Development of omniphobic desalination membranes using a charged electrospun nanofiber scaffold, ACS Appl. Mater. Interfaces 8 (2016) 11154–11161, http://dx.doi.org/10.1021/acsami. 6b02419.
- [37] Y.G. Zmievskii, Determination of critical pressure in membrane distillation process,

- Pet. Chem. 55 (2015) 308–314, http://dx.doi.org/10.1134/S0965544115040118.
 38] N.V. Churaev, G.A. Martynov, V.M. Starov, Z.M. Zorin, Some features of capillary imbibition of surfactant solutions, Colloid Polym. Sci. 259 (1981) 747–752.
- [39] V.M. Starov, S.A. Zhdanov, M.G. Velarde, Capillary imbibition of surfactant solutions in porous media and thin capillaries: partial wetting case, J. Colloid Interface Sci. 273 (2004) 589–595, http://dx.doi.org/10.1016/j.jcis.2004.02.033.
- [40] M.S. Romero-Cano, A. Martín-Rodríguez, F.J. de las Nieves, Adsorption and desorption of triton X-100 in polystyrene particles with different functionality: i. Adsorption study, J. Colloid Interface Sci. 227 (2000) 322–328, http://dx.doi.org/10.1006/jcis.2000.6862.
- [41] M.S. Romero-Cano, A. Martín-Rodríguez, F.J. de las Nieves, Adsorption and desorption of triton X-100 in polystyrene particles with different functionality: I. Adsorption study, J. Colloid Interface Sci. 227 (2000) 322–328, http://dx.doi.org/10.1006/jcis.2000.6862
- [42] A. Martín-Rodríguez, M.A. Cabrerizo-Vílchez, R. Hidalgo-Álvarez, A comparative study on the adsorption of Triton X-100 and Tween 20 onto latexes with different interfacial properties, J. Colloid Interface Sci. 187 (1997) 139–147, http://dx.doi. org/10.1006/jcis.1996.4681.
- [43] J. Landers, G.Y. Gor, A.V. Neimark, Colloids Surf.: Physicochem. Eng. Asp. 437 (2013) 3–32, http://dx.doi.org/10.1016/j.colsurfa.2013.01.007.
- [44] J.D. Berry, M.J. Neeson, R.R. Dagastine, D.Y.C. Chan, R.F. Tabor, Measurement of surface and interfacial tension using pendant drop tensiometry, J. Colloid Interface Sci. 454 (2015) 226–237, http://dx.doi.org/10.1016/j.jcis.2015.05.012.
- [45] M.G. Cabezas, A. Bateni, J.M. Montanero, A.W. Neumann, A new drop-shape methodology for surface tension measurement, Appl. Surf. Sci. (2004) 480–484, http://dx.doi.org/10.1016/j.apsusc.2004.05.250.
- [46] Z. Wang, D. Hou, S. Lin, Composite membrane with underwater-oleophobic surface for anti-oil-fouling membrane distillation, Environ. Sci. Technol. (2016), http://dx. doi.org/10.1021/acs.est.5b05976 (acs.est.5b05976).
- [47] J.C. Tuberquia, W.S. Song, G.K. Jennings, Investigating the superhydrophobic behavior for underwater surfaces using impedance-based methods, Anal. Chem. 83 (2011) 6184–6190, http://dx.doi.org/10.1021/ac200650z.
- [48] J.C. Tuberquia, N. Nizamidin, G.K. Jennings, Effect of superhydrophobicity on the barrier properties of polymethylene films, Langmuir 26 (2010) 14039–14046, http://dx.doi.org/10.1021/la102312w.
- [49] B.J. Kirby, Micro- and nanoscale fluid mechanics: transport in microfluidic devices, Brian (2010) 512, http://dx.doi.org/10.1007/s13398-014-0173-7.2.
- [50] H. Bruus, Theoretical microfluidics, Physics 18 (2008) 363, http://dx.doi.org/10. 1111/i.1574-6968.2009.01808.x.
- [51] K. Streletzky, G.D.J. Phillies, Temperature dependence of triton X-100 micelle size and hydration, Langmuir 11 (1995) 42–47, http://dx.doi.org/10.1021/ la00001a011.
- [52] H.H. Paradies, Shape and size of a nonionic surfactant micelle. Triton X-100 in aqueous solution, J. Phys. Chem. 84 (1980) 599–607, http://dx.doi.org/10.1021/ j100443a008.